Supporting Information

Mao et al. 10.1073/pnas.1307382110

SI Materials and Methods

Protein Expression and Purification. Details of HIV-1 Env expression and purification have been described previously (1). In brief, *env* DNA encoding the HIV-1_{JR-FL} membrane-bound HIV-1 Env trimer [Env(-)ΔCT] glycoprotein was codon-optimized and subcloned into the pcDNA3.1(-) expression plasmid (Invitrogen). The Env(-)ΔCT glycoprotein was transiently expressed in 293F cells. Thirty-six hours after transfection, cells expressing the envelope glycoproteins were harvested by spinning the cell suspension at 100 × *g* for 5 min at 4 °C, followed by washing with PBS at 4 °C. The cell pellets were resuspended in approximately five volumes of homogenization buffer [250 mM sucrose, 10 mM Tris·HCl (pH 7.4), and a mixture of protease inhibitors (Roche Complete tablets)]. The resuspended cells were homogenized in a 50-mL glass Dounce homogenizer on ice. The homogenate was spun at 600 × *g* for 10 min at 4 °C. The pellet was discarded, and the supernatant was collected and spun at 8,000 × *g* for 10 min at 4 °C. The supernatant solution was collected and was ultracentrifuged at 100,000 × *g* for 30 min at 4 °C. The pellet containing plasma membranes was collected and the supernatant discarded. The pellet was resuspended in homogenization buffer and was homogenized in a 15-mL glass Dounce homogenizer and ultracentrifuged at 100,000 × *g* for 45 min at 4 °C. The pellet containing purified plasma membrane was collected and solubilized in a solubilization buffer containing 100 mM $(NH_4)_2SO_4$, 20 mM Tris·HCl (pH 8), 300 mM NaCl, 20 mM imidazole, 1% (wt/vol) Cymal-5 (Affymetrix), and a mixture of protease inhibitors (Roche Complete tablets). The membranes were solubilized by incubation at 4 °C for 30 min on a rocking platform. The suspension was ultracentrifuged for 30 min at 200,000 × *g* at 4 °C. The supernatant was collected and mixed with a small volume of preequilibrated Ni-NTA beads (Qiagen) for 8–12 h on a rocking platform at 4 C°. The mixture was then injected into a small column and washed with a buffer containing 100 mM $(NH_4)_2SO_4$, 20 mM Tris·HCl (pH 8), 1 M NaCl, 30 mM imidazole, 0.5% Cymal-5 (for 1-mL Ni-NTA beads, we used ∼15–30 mL buffer for washing). The well-washed bead-filled column was eluted with a buffer containing 100 mM $(NH_4)_2SO_4$, 20 mM Tris·HCl (pH 7.4), 250 mM NaCl, 250 mM imidazole, and 0.5% Cymal-5. The eluted Env(-)ΔCT glycoprotein solution was concentrated, diluted in a buffer containing 20 mM Tris·HCl (pH 7.4), 300 mM NaCl, and 0.01% Cymal-6, and reconcentrated to 1.5–2.5 mg/mL before cryo-sample preparation.

Cryo-EM Data Collection. To prepare the cryo-sample for single-particle imaging, 2.5 μL of the 1.5–2.5 mg mL^{-1} Env(-)ΔCT solution was spread on a C-flat holey carbon grid (Electron Microscopy Sciences) in a chamber of 100% humidity, held for 2 s, blotted with filter paper for 2 s at 4 °C, and then flash-plunged into liquid ethane by Vitrobot (FEI). The prepared cryo-grids were transferred into the CT3500 cryo-transfer system (Gatan) in liquid nitrogen and were used for single-particle image data collection at −183 °C. Focus pairs of micrographs were recorded on a Tecnai F20 TEM (FEI) with a field-emission gun at 200 kV and a calibrated magnification of 200,835× on a 4k × 4k Ultrascan CCD camera (Gatan). The electron dose of each exposure was 10–15 electrons $Å^{-2}$. The defocus of the second set of micrographs differed from that of the first set by 1.0 μm. The majority of accumulated image data were collected with the assistance of the Leginon automated imaging system (2) in a semiautomatic fashion.

Image Processing and 3D Reconstruction. Micrographs were screened for drift, astigmatism, and visibility of Thon rings in the power spectra. Parameters of the contrast transfer function (CTF) of each micrograph were determined with the CTFFind3 program (3, 4). A total of 670,000 single-particle images (with dimensions of 256 × 256 pixels and a pixel size of 0.747 Å) selected from the closer-to-focus micrographs were used for structure refinement. The defocus ranged from −350 to −3,000 nm. The quality and selection of these particle images were evaluated and verified comprehensively by unsupervised classification using multivariate data analysis and K-means clustering, as previously described (5). Each single-particle image was decimated by 4 times to a dimension of 64 × 64 pixels, and was low-pass filtered at 12 Å for particle verification. The initial alignment for projection Euler angles and in-plane shift was generated by the projection-matching algorithm using a previously determined 11-Å map of the same Env construct as an initial reference (Electron Microscopy Data Bank accession code: EMD-5418). The particles images were grouped into 57 defocus groups, with a defocus width of 20 nm in each group before refinement. The back-projection reconstruction at each iteration of the refinement was CTF-corrected by Wiener filtering (6, 7). The angular increment was progressively decreased from 10° to 0.5° in the refinement. The resolution of the reconstruction was measured by both conventional Fourier shell correlation (FSC) (8, 9) and the "gold-standard" FSC (10, 11). The latter was calculated by two half datasets that were refined fully independently from each other, keeping all but the initial reference separate (10). The former approach estimated a final resolution of 5.5 Å by conventional FSC at 0.5 cutoff, and the latter approach estimated a final resolution of 6 Å by the "gold-standard" FSC at 0.5 cutoff. The final map obtained by the "gold standard" refinement protocol was deconvoluted and amplitude-corrected by a B-factor of −150 $Å^2$ and was low-pass filtered at 5.8 Å with a cosine edge of 8-Fourier-pixel width (12, 13). The above image analysis was implemented in customized computational procedures and workflows, combining the functions of SPIDER (14) and XMIPP (15).

Structure Analysis. Segmentation of the cryo-EM density was done in University of California, San Francisco (UCSF) Chimera (16). Fitting of crystal structures and secondary structure elements in the cryo-EM map was performed in O (17) and Coot (18). The secondary structure elements of the glycoprotein (gp)120 inner domain were positioned by flexibly fitting the crystal structure of the CD4-bound gp120 core [Protein Data Bank (PDB) ID: 3JWD] to the cryo-EM map by the Flex-EM program (1), based on molecular dynamics simulations in Modeler (20) and by energetic optimization in CNS (21). Analysis of CD4BS antibody interaction with the Env trimer was done by fitting the gp120 outer domain from the antibody:gp120 core complex crystal structure to the cryo-EM map in a rigid-body fashion in Coot and UCSF Chimera. Graphics were done in PyMOL (Schrodinger) and UCSF Chimera.

Cell-Based ELISA. Ligand binding to trimeric envelope glycoproteins on the surface of COS-1 or HOS.pBABEpuro cells [ATCC and National Institutes of Health (NIH) AIDS Research and Reference Reagent Program, respectively] was measured by a cell-based ELISA, as previously described (22). In brief, COS-1 or HOS cells were seeded in 96-well plates (2×10^4 cells per well) and transfected the next day with 0.15 μg per well of plasmid DNA expressing the codon-optimized (GenScript) genes encoding the HIV-1_{JR-FL} wild-type Env, Env(+)ΔCT (cleavage-competent,

cytoplasmic tail-deleted) and Env(-)ΔCT (cleavage-negative, cytoplasmic tail-deleted) glycoproteins using the standard polyethylenimine (PEI; Polyscience) transfection method. The Env proteolytic cleavage site was altered by R508S and R511S changes; the Env cytoplasmic tail was truncated by substitution of a stop codon for codon 712. Two days after the transfection, the cells were washed twice with blocking buffer [10 mg/mL nonfat dry milk, 1.8 mM $CaCl_2$, 1 mM $MgCl_2$, 25 mM Tris (pH 7.5), and 140 mM NaCl] and then incubated for 1 h at room temperature with Env ligands. The ligands tested were polyclonal antibodies in a pool of heat-inactivated sera from HIV-1–infected individuals (used at 1/2,000 dilution); a 1-μg/mL dilution of CD4-Ig [a fusion protein in which the N-terminal two domains of CD4 are linked to the Fc component of IgG (23)]; or anti-HIV-1 Env monoclonal antibodies VRC01, b12, b13, F105, 17b, 2G12, 2F5, 4e10, A32, C11, PGT121, and PGT126 at a 1-μg/mL dilution. An HRP-conjugated antibody specific for the Fc region of human IgG (Pierce) was then incubated with the samples for 45 min at room temperature. Cells were washed five times with blocking buffer and five times with washing buffer. HRP enzyme activity was determined after the addition of 30 μL per well of a 1:1 mix of Western Lightning oxidizing and luminol reagents (Perkin-Elmer Life Sciences). Light emission was measured with an LB 941 TriStar luminometer (Berthold Technologies). The following reagents were obtained through the NIH AIDS Research and Reference Reagent Program, Division of AIDS, National Institute of Allergy and Infectious Diseases, NIH: monoclonal antibodies to HIV-1 gp41 (98-6, 126-7, 246-D, 240-D, 50-69) from S. Zolla-Pazner; HIV-1 gp41 monoclonal antibodies (4E10, 5F3) from H. Katinger; and HIV-1 gp41 monoclonal antibody (F240) from M. Posner and L. Cavacini.

1. Mao Y, et al. (2012) Subunit organization of the membrane-bound HIV-1 envelope glycoprotein trimer. *Nat Struct Mol Biol* 19(9):893–899.
2. Suloway C, et al. (2005) Automated molecular microscopy: The new Leginon system. *J Struct Biol* 151(1):41–60.
3. Huang Z, Baldwin PR, Mullapudi S, Penczek PA (2003) Automated determination of parameters describing power spectra of micrograph images in electron microscopy. *J Struct Biol* 144(1-2):79–94.
4. Mindell JA, Grigorieff N (2003) Accurate determination of local defocus and specimen tilt in electron microscopy. *J Struct Biol* 142(3):334–347.
5. Shaikh TR, Trujillo R, LeBarron JS, Baxter WT, Frank J (2008) Particle-verification for single-particle, reference-based reconstruction using multivariate data analysis and classification. *J Struct Biol* 164(1):41–48.
6. Frank J (2006) *Three-Dimensional Electron Microscopy of Macromolecular Assemblies: Visualization of Biological Molecules in Their Native State* (Oxford Univ Press, Oxford).
7. Penczek PA (2010) Image restoration in cryo-electron microscopy. *Methods Enzymol* 482:35–72.
8. Penczek PA (2010) Resolution measures in molecular electron microscopy. *Methods Enzymol* 482:73–100.
9. Liao HY, Frank J (2010) Definition and estimation of resolution in single-particle reconstructions. *Structure* 18(7):768–775.
10. Grigorieff N (2000) Resolution measurement in structures derived from single particles. *Acta Crystallogr D Biol Crystallogr* 56(Pt 10):1270–1277.
11. Scheres SHW, Chen S (2012) Prevention of overfitting in cryo-EM structure determination. *Nat Methods* 9(9):853–854.
12. Rosenthal PB, Henderson R (2003) Optimal determination of particle orientation, absolute hand, and contrast loss in single-particle electron cryomicroscopy. *J Mol Biol* 333(4):721–745.
13. Fernández JJ, Luque D, Castón JR, Carrascosa JL (2008) Sharpening high resolution information in single particle electron cryomicroscopy. *J Struct Biol* 164(1):170–175.
14. Shaikh TR, et al. (2008) SPIDER image processing for single-particle reconstruction of biological macromolecules from electron micrographs. *Nat Protoc* 3(12):1941–1974.
15. Scheres SHW, Núñez-Ramírez R, Sorzano COS, Carazo JM, Marabini R (2008) Image processing for electron microscopy single-particle analysis using XMIPP. *Nat Protoc* 3(6):977–990.
16. Pettersen EF, et al. (2004) UCSF Chimera—a visualization system for exploratory research and analysis. *J Comput Chem* 25(13):1605–1612.
17. Jones TA (2004) Interactive electron-density map interpretation: From INTER to O. *Acta Crystallogr D Biol Crystallogr* 60(Pt 12 Pt 1):2115–2125.
18. Emsley P, Lohkamp B, Scott WG, Cowtan K (2010) Features and development of Coot. *Acta Crystallogr D Biol Crystallogr* 66(Pt 4):486–501.
19. Topf M, et al. (2008) Protein structure fitting and refinement guided by cryo-EM density. *Structure* 16(2):295–307.
20. Martí-Renom MA, et al. (2000) Comparative protein structure modeling of genes and genomes. *Annu Rev Biophys Biomol Struct* 29:291–325.
21. Brunger AT (2007) Version 1.2 of the Crystallography and NMR system. *Nat Protoc* 2(11):2728–2733.
22. Haim H, et al. (2009) Soluble CD4 and CD4-mimetic compounds inhibit HIV-1 infection by induction of a short-lived activated state. *PLoS Pathog* 5(4):e1000360.
23. Herschhorn A, Marasco WA, Hizi A (2010) Antibodies and lentiviruses that specifically recognize a T cell epitope derived from HIV-1 Nef protein and presented by HLA-C. *J Immunol* 185(12):7623–7632.

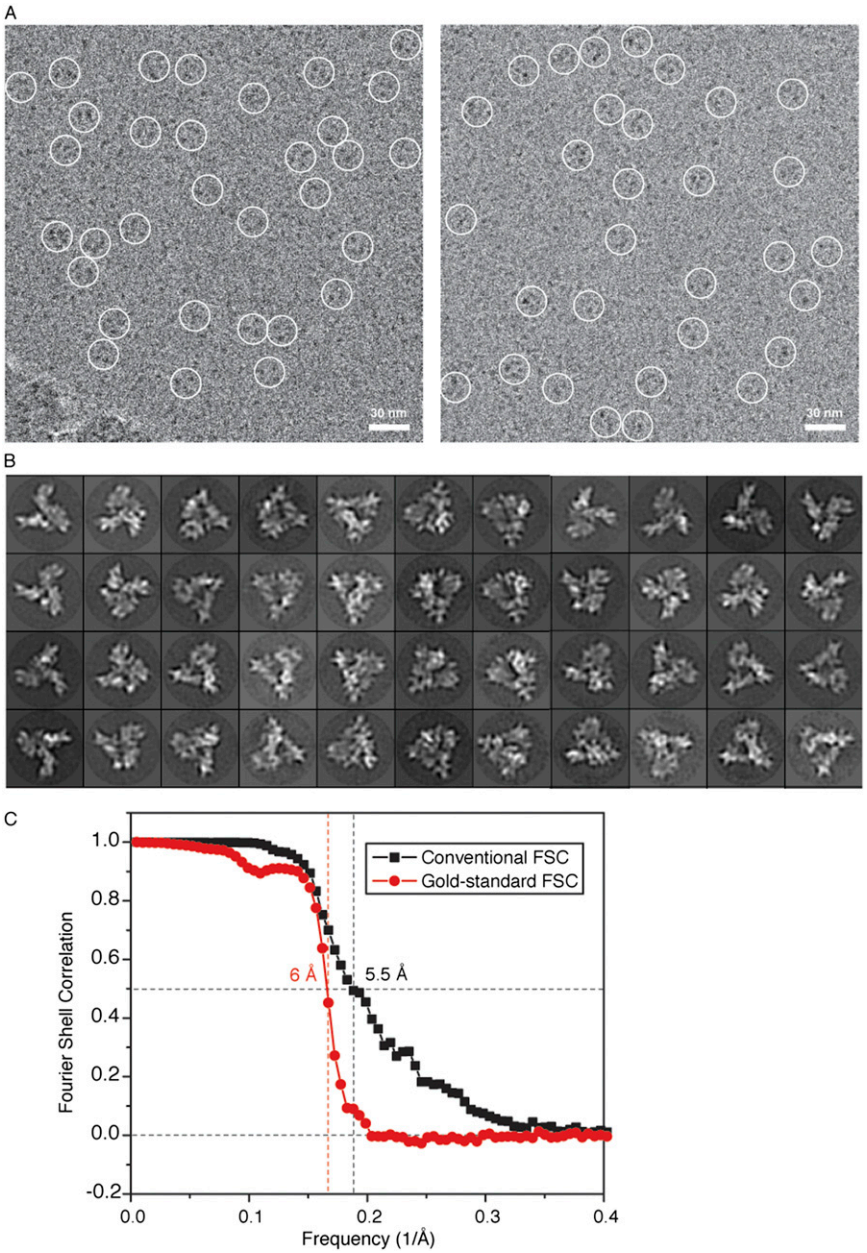

Fig. S1. Cryo-EM imaging and resolution assessment. (*A*) Two typical 4k × 4k micrographs of the purified HIV-1_{JR-FL}Env(-)ΔCT trimers protected by the Cymal-6 detergent and embedded in a vitreous ice film. The micrograph shown is low-pass filtered at 1.0 nm. A number of candidate single-particle projections of the Env trimer are highlighted by white circles. Defocus of the micrograph is ~3 μm. (*B*) Gallery of selected typical class-average images after initial alignment and 2D refinement. Note the improved structural details not evident in the raw images and not apparent in the previously reported lower-resolution model (1). (*C*) Resolution measurement of the cryo-EM structure of the HIV-1_{JR-FL}Env(-)ΔCT trimer, using both the conventional FSC approach at FSC-0.5 cutoff and the gold standard FSC approach at 0.5 cutoff. The conventional FSC (black curve) was calculated between two separate reconstructions, each generated from a randomly divided half of the entire dataset, both of which were refined with a single common reference. The gold standard FSC (red curve) was calculated between two half-set reconstructions that were refined independently with two fully separate references. The conventional FSC at 0.5 cutoff yielded a slightly higher estimate of resolution compared with the gold standard FSC at 0.5 cutoff. The reported resolution is based on the gold standard FSC approach.

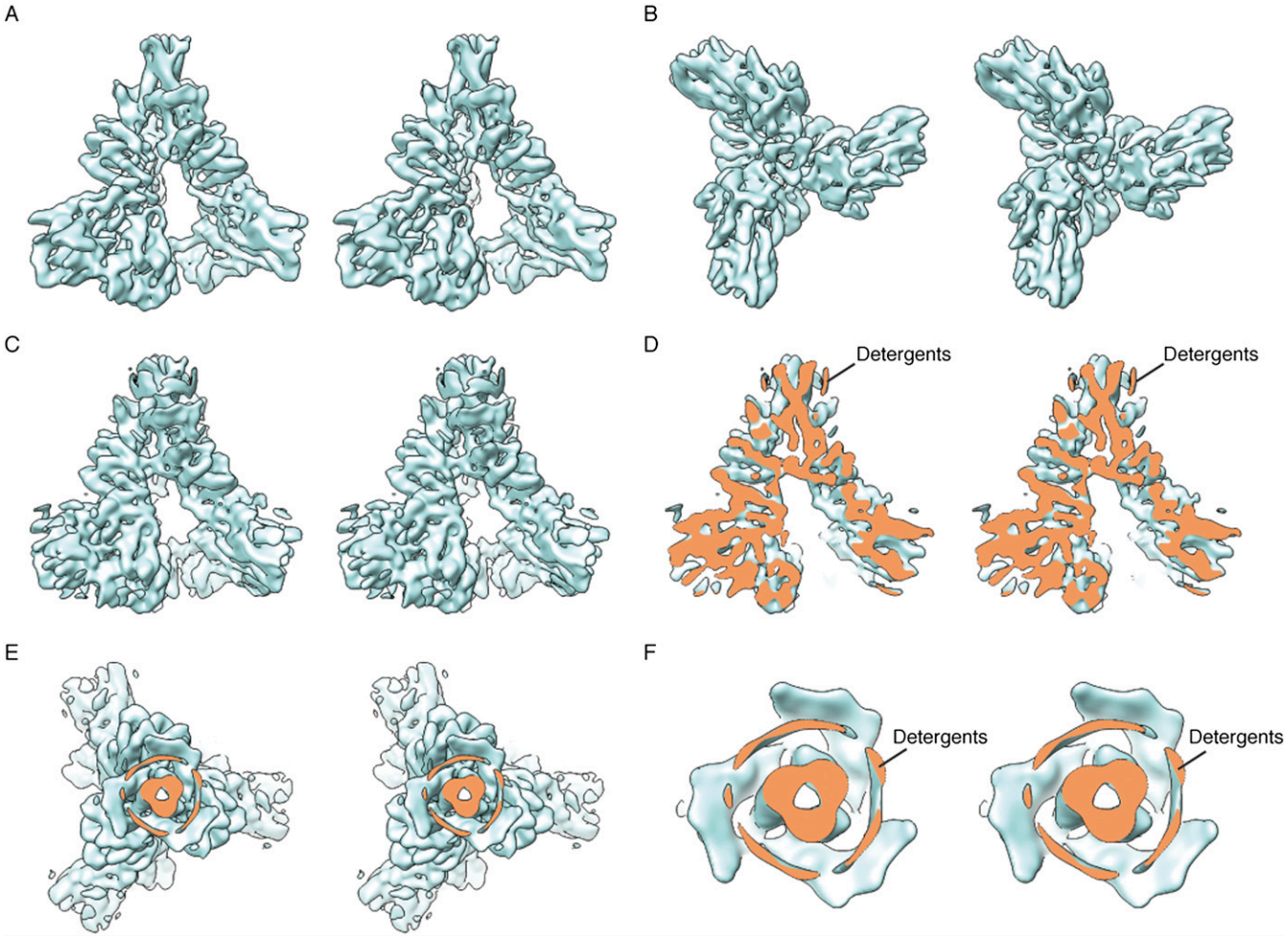

Fig. S2. Stereo views of the overall cryo-EM structure of the HIV-1_{JR-FL}Env trimer. (*A*) Stereo view of the cryo-EM map in an isosurface representation, viewed from a perspective parallel to the viral membrane. (*B*) Stereo view of the same isosurface, viewed from the perspective of the target cell. (*C*) Stereo view of the cryo-EM map in an isosurface representation at a lower level of contour compared with that in *A* and *B*, viewed from a perspective parallel to the viral membrane. (*D*) Stereo view of the same isosurface as that shown in *C*, with its central cross-section clipped. (*E*) Stereo view of the cryo-EM map in the same isosurface representation as that shown in *C*, viewed from a perspective from the interior of the virus, with the cross-section of the transmembrane region clipped. (*F*) Stereo view of a close-up of the cross-section of the transmembrane region, showing three separated thin layers, which likely represent detergent molecules surrounding the transmembrane helices.

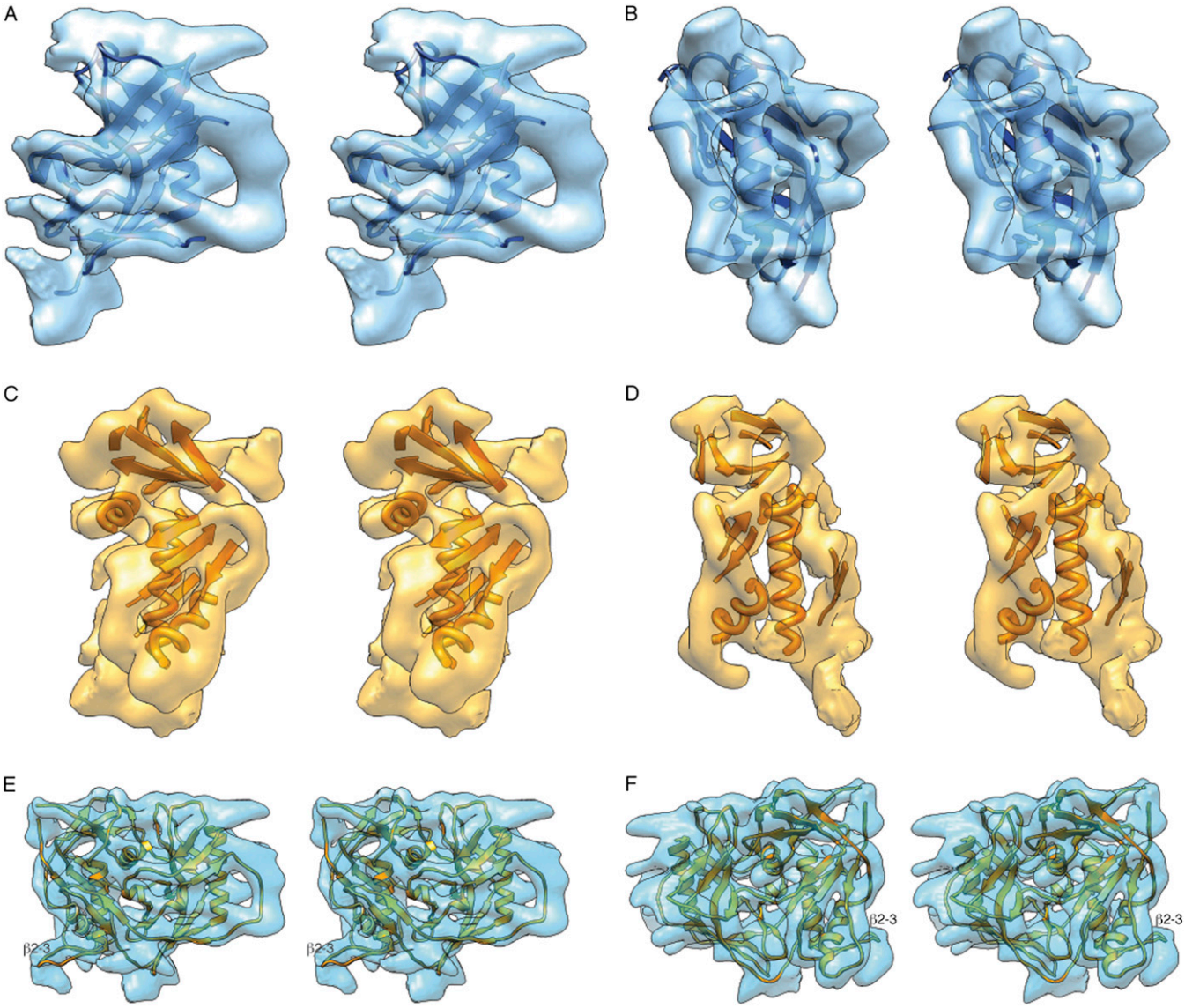

Fig. S3. Stereo views of the unliganded gp120 core structure fitted in the cryo-EM map. (*A*) Cryo-EM density segment associated with the gp120 outer domain is shown as a transparent isosurface. The crystal structure of the outer domain of the gp120 core is fitted into the cryo-EM density as a rigid body and is shown in ribbon representation. (*B*) Same isosurface as shown in *A*, rotated 90° around the vertical axis. The density associated with the gp120 V4 variable loop, which was not resolved in the crystal structure, is evident on the right-hand side of the molecule in *A* and projects toward the viewer in *B*. (*C*) The cryo-EM density segment associated with the gp120 inner domain is shown as a transparent isosurface. The secondary structure of the gp120 inner domain was assessed by flexible fitting, and the approximate positions of secondary structure elements are shown in cartoon representation. (*D*) Stereo view of the same density as in *C*, rotated 90° around the vertical axis. (*E* and *F*) Crystal structure of the gp120 core was flexibly fitted into the cryo-EM density segment associated with the overall gp120 core, from two opposite perspectives.

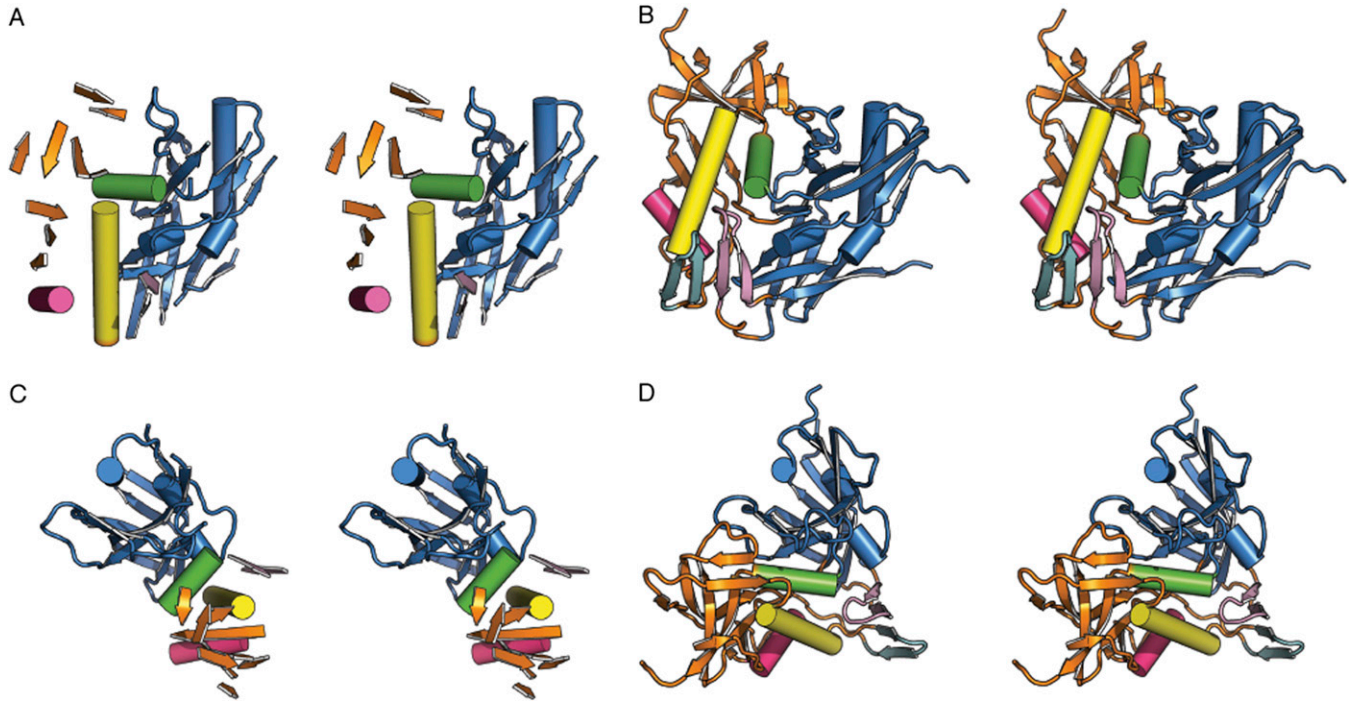

Fig. S4. Stereo views of the comparison between the conformations of the unliganded gp120 core in the Env trimer and the monomeric CD4-bound gp120 core. (*A* and *C*) Stereo views of the secondary structures in the gp120 core that was flexibly fitted to the unliganded state of the Env trimer. (*B* and *D*) Stereo views of a ribbon representation of the CD4-bound monomeric gp120 core (PDB ID: 3JWD). For comparison between the unliganded state and the CD4-bound state, the gp120 outer domains (blue) are aligned in the same orientation between *A* and *B*, and between *C* and *D*. The view in *A* and *B* is from a perspective roughly parallel to the viral membrane. The view in *C* and *D* is from the perspective of the viral membrane.

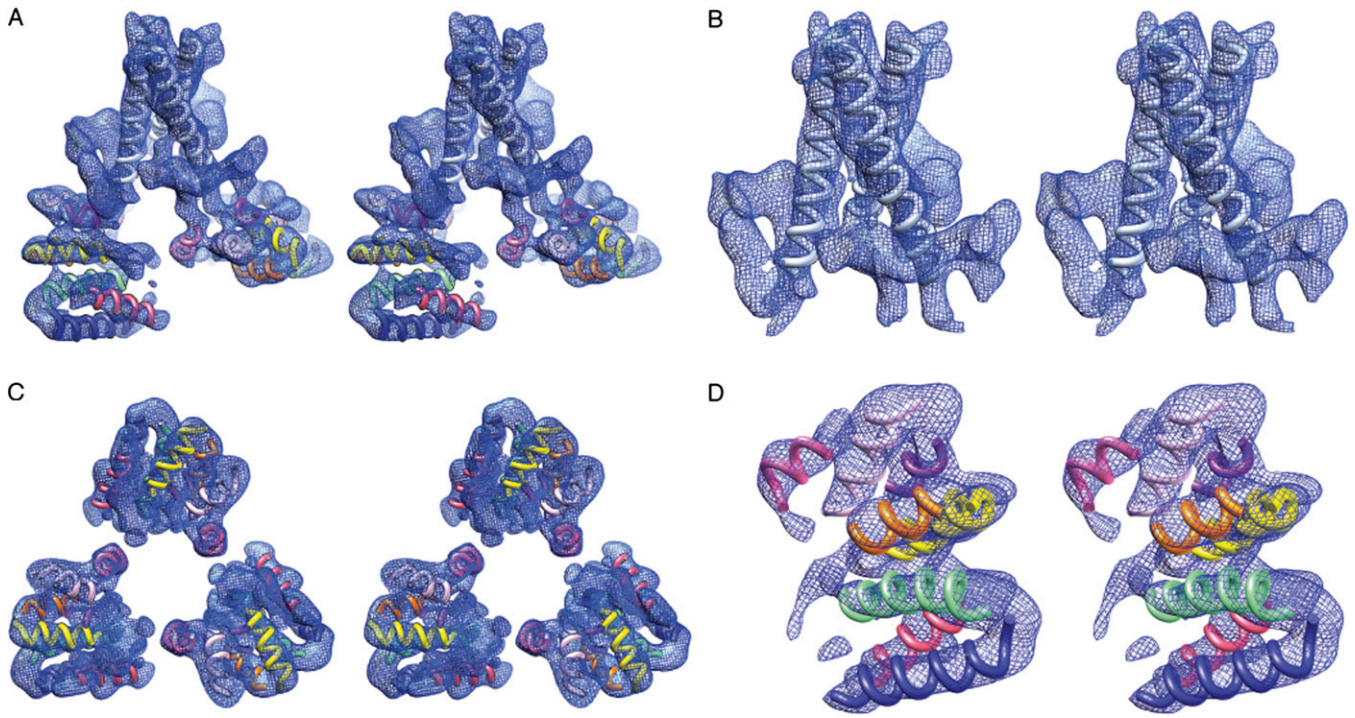

Fig. S5. Stereo views of the gp41 structure. (*A*) Stereo view of the density associated with the three gp41 subunits in the Env trimer, viewed from an angle of 30° with respect to the viral membrane. (*B*) Stereo view of the segmented density of the gp41 membrane-interactive region, viewed from the same perspective as that in *A*. (C) Stereo view of the density associated with the gp41 ectodomain, viewed from the perspective of the viral membrane. (*D*) Stereo view of the gp41 ectodomain, from a perspective parallel to the viral membrane.

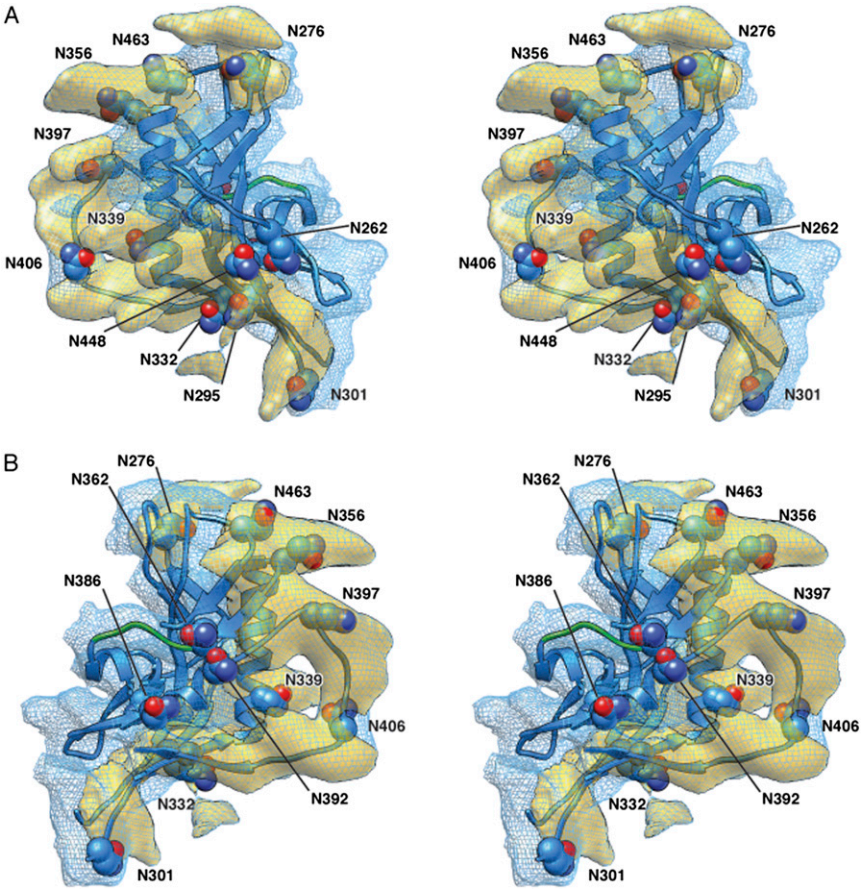

Fig. S6. Stereo views of gp120 glycan-associated density. (*A*) Stereoview of the glycan-associated densities on the gp120 surface, viewed from a perspective parallel to the viral membrane. The gp120 outer domain ribbon is colored blue, and the asparagine residues associated with potential *N*-linked glycosylation sites are depicted in Corey-Pauling-Koltun (CPK) representation and labeled. (*B*) Stereo view of the glycan-associated densities on the gp120 surface. The perspective is ~180° from that of *A*. These images reproduce Fig. 5 in stereo. The yellow densities highlight the glycan-associated cryo-EM segments.

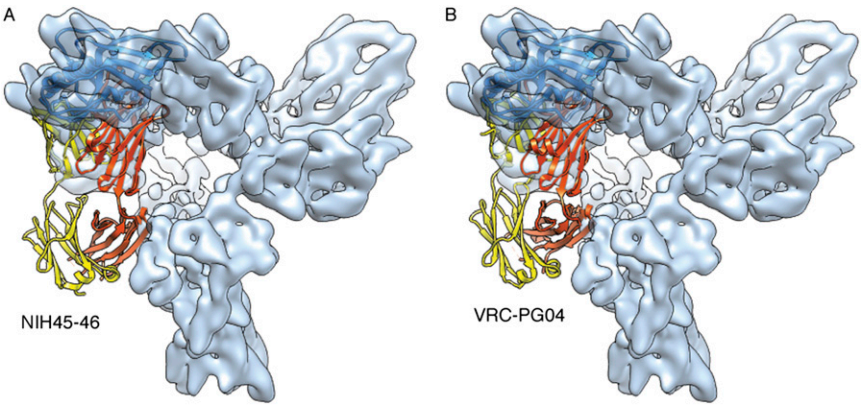

Fig. S7. Additional CD4BS antibody interactions with the Env trimer. Crystal structures of the gp120 core in complex with the CD4BS antibodies, NIH45-46 (*A*) and VRC-PG04 (*B*), were superposed on the unliganded Env trimer map as follows: the conformationally rigid gp120 outer domain was fitted to the Env trimer density map, and the outer domains in the crystal structures were aligned with the fitted outer domain (represented as a blue ribbon). These figures are an extension of Fig. 6, with the complexes viewed from the perspective shown in that figure. The PDB IDs of the antibodies in complex with gp120 core structures are 3U7Y (*A*) and 3SE9 (*B*).

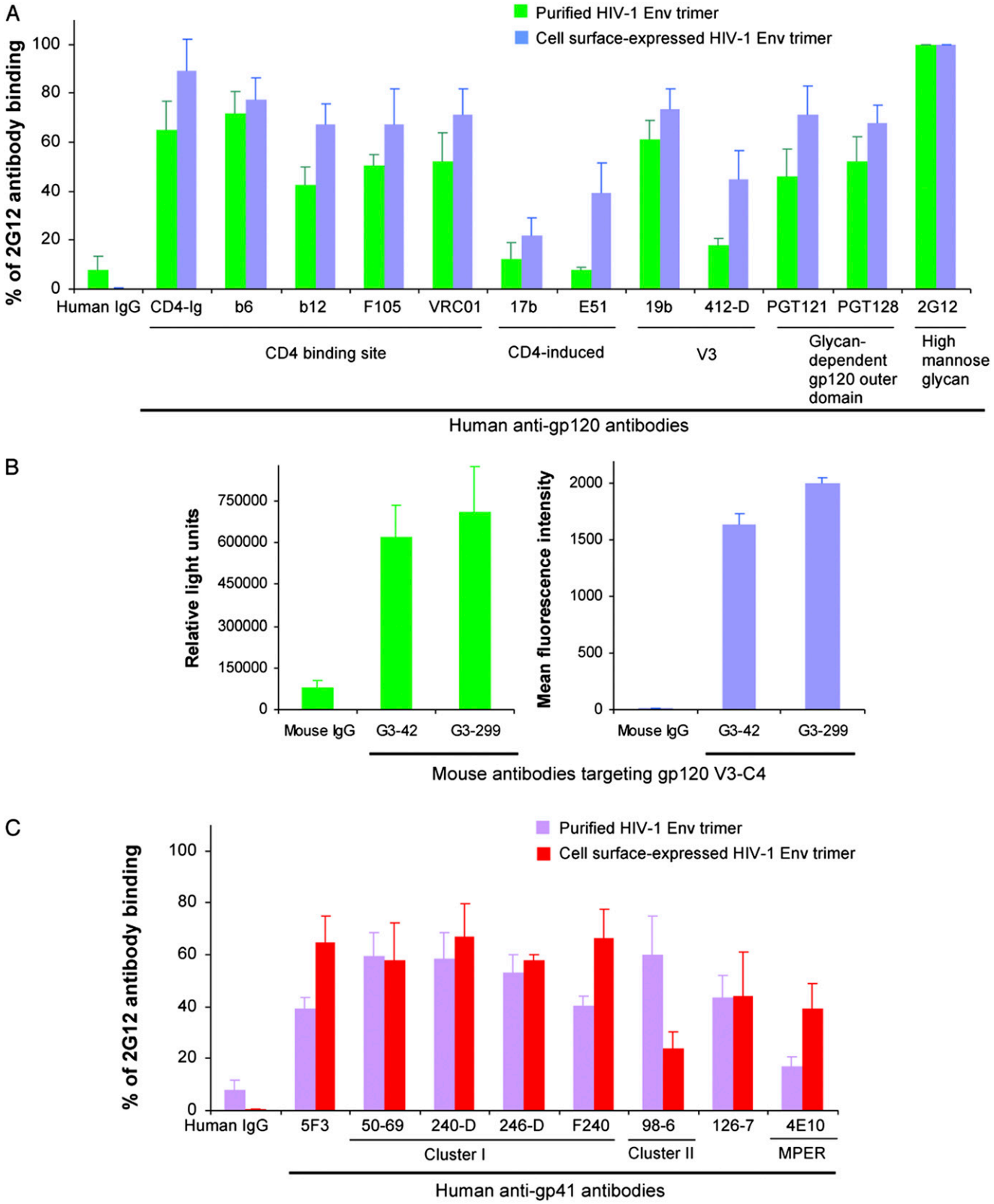

Fig. S8. Antigenic profile of the purified HIV-1 envelope trimer. The structural integrity of the purified HIV-1_{JR-FL}Env(-)ΔCT trimer was evaluated by testing the binding at 20 °C of a large panel of monoclonal antibodies and CD4-Ig to the purified trimer in an ELISA. Binding of the same ligands to an identical HIV-1_{JR-FL}Env(-)ΔCT trimer expressed transiently on the surface of transfected cells was measured at 20 °C by flow cytometry and served as a reference. Under the conditions of these experiments [and in contrast to the modeling of the fixed Env(-)ΔCT trimer in Fig. 6], the Env(-)ΔCT glycoprotein can undergo conformational changes during incubation with the antibody. (*A*) Binding of conformation-dependent antibodies to the indicated epitopes on HIV-1 gp120. (*B*) Binding of mouse antibodies directed against conformation-dependent epitopes comprising the V3 region and the fourth conserved region (C4) of HIV-1 gp120. Antibody binding to detergent-solubilized, purified Env(-)ΔCT glycoprotein (green) and Env(-)ΔCT glycoprotein expressed on cell surfaces (blue) is

Legend continued on following page

shown. (C) Binding of antibodies to different regions on HIV-1 gp41. Each ligand was tested at a single concentration of 10 μg/mL, and polyclonal human IgG (or mouse IgG) served as a negative control. The mean fluorescence intensity associated with the binding of the polyclonal human and mouse IgG negative controls to the cell surface-expressed Env was too low to be seen on the bar graph. Results shown represent the average of three independent experiments. V3, the third variable loop of gp120; C4, the fourth conserved region of gp120; cluster I, gp41 amino acids 597–613; cluster II, gp41 amino acids 644–663; MPER, membrane-proximal external region.

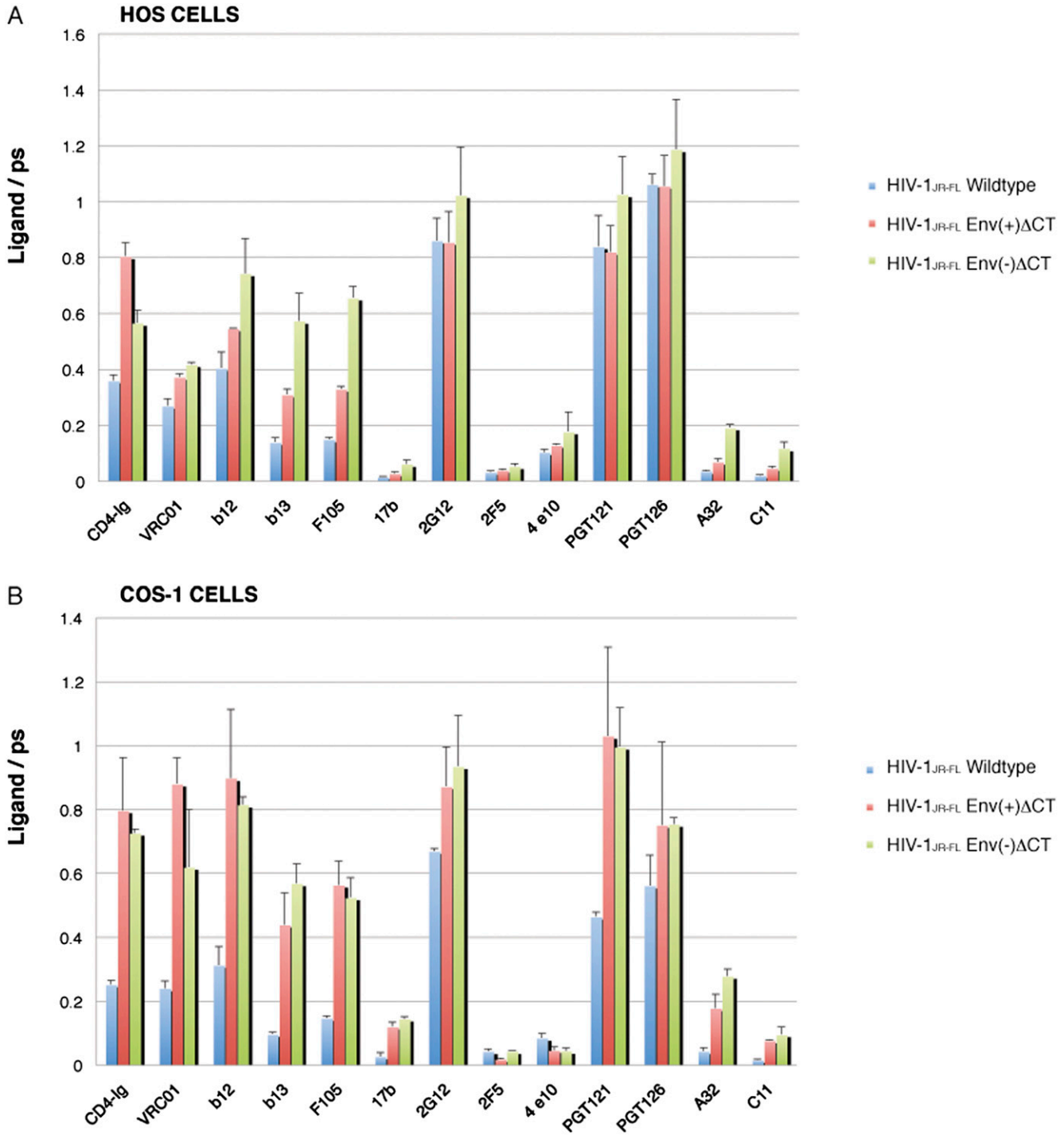

Fig. S9. Binding of cell-surface HIV-1_{JR-FL}Env variants by Env ligands. The binding of Env ligands (CD4-Ig and monoclonal antibodies) was measured to three HIV-1_{JR-FL}Env variants: wild-type Env; Env(+)ΔCT (intact proteolytic cleavage site, truncated cytoplasmic tail), and Env(-)ΔCT (modified proteolytic cleavage site, truncated cytoplasmic tail), using a cell-based ELISA. The Env variants were expressed in transfected HOS (*A*) or COS-1 (*B*) cells. Proteolytic cleavage of the wild-type Env and Env(+)ΔCT glycoproteins was more efficient in HOS cells than in COS-1 cells. The Env ligands were CD4-Ig, CD4-binding site antibodies (VRC01, b12, b13, F105), a CD4-induced antibody (17b), glycan-dependent antibodies (2G12, PGT121, PGT126), an inner domain-specific antibody (A32), an antibody against the gp120 N/C termini (C11), and antibodies against the gp41 MPER (2F5, 4E10). Results were normalized to the signal obtained with pooled sera (ps) from HIV-1–infected individuals. Results are representative of at least two independent experiments, each performed in duplicate.

Table S1. Quantitative evaluation of the goodness of fit

Parameter	No. of residues in the density	No. of residues out of the density	No. of total residues fitted	Goodness of fit (%)
Rigid-body fit of gp120 outer domain	127	14	141	90
Flexible fit of gp120 outer domain	150	1	151	99.3
Flexible fit of gp120 inner domain	190	4	194	98
Flexible fit of gp120 core	340	5	345	98.6
Gp120 TAD helix	12	0	12	100
Gp41 helix 1	28	0	28	100
Gp41 helix 2	5	0	5	100
Gp41 helix 3	10	0	10	100
Gp41 helix 4	5	0	5	100
Gp41 helix 5	10	0	10	100
Gp41 helix 6	16	1	17	94
Gp41 helix 7	16	0	16	100
Gp41 helix 8	17	0	17	100
Gp41 helix 9	15	0	15	100

The contour level of the density used to assess the fit is 2σ. The goodness of fit is indicated as the percent of the backbone residues inside the density. The side-chain fit was not taken into account in the evaluation. The numbering of gp41 helices is roughly proportional to their distance from the C terminus of the transmembrane region.

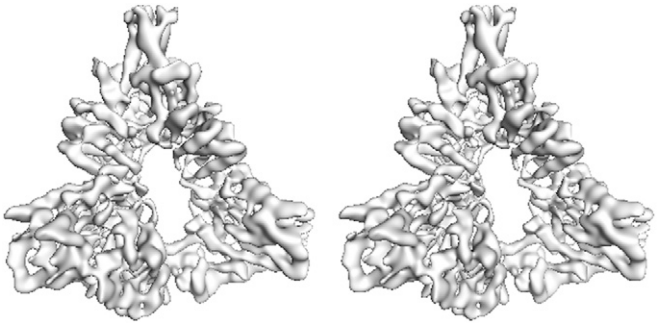

Movie S1. Side-by-side 3D movie showing the cryo-EM map of the unliganded HIV-1 envelope glycoprotein trimer. The cryo-EM density is shown at 3σ level.

Movie S1

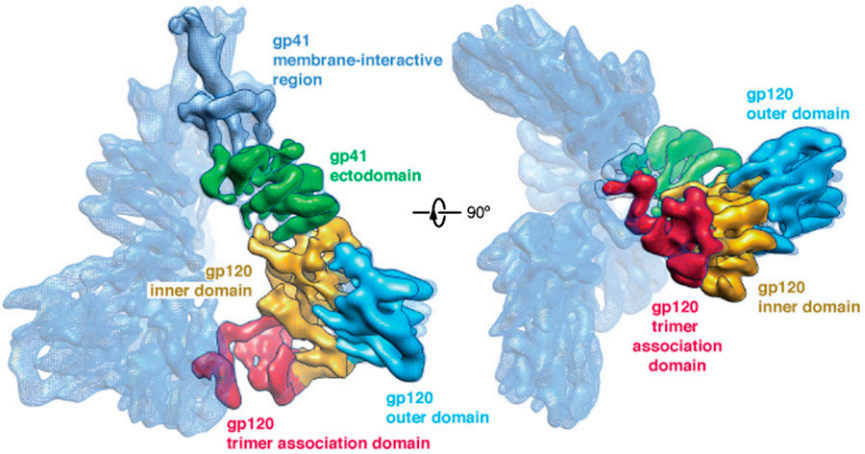

Movie S2. Side-by-side 3D movie showing the domain-based map segmentation of the cryo-EM structure of the unliganded HIV-1 envelope glycoprotein trimer.

Movie S2